Design and Fabrication of E-band Traveling Wave Tube for High Data Rate Wireless Links

Claudio Paoloni *Senior Member, IEEE*, Rupa Basu, *Student, IEEE*, Purushothaman Narasimhan, Jonathan Gates and Rosa Letizia *Senior Member, IEEE*

Abstract— **E-band (71 - 76 GHz and 81 - 86 GHz) is widely used for wireless point to point links with a few Gigabit/second data rate. E-band front-ends are powered by solid state amplifiers with about 1 W output power per module. This level of output power limits range and spectral efficiency in rain condition and has to be compensated by high gain antennas or backup low frequency links with reduced capacity. The availability of tens of Watts of transmission power would allow higher spectral efficiency and long range, and the use of lower gain antennas for multibeam and area coverage.**

Millimeter wave Traveling Wave Tubes (TWTs) are gaining interest due to their higher power, more than one order of magnitude, in comparison to solid state devices. Helix TWTs, typically built at microwaves, are very arduous to fabricate due to the extremely small diameter of an helix at E-band.

This paper reports the design and fabrication of the first ever E-band TWT based on a full metal slow wave structure, the double corrugated waveguide. The TWT is designed to provide about 70 W power and more than 35 dB gain in the 71 - 76 GHz band. A test TWT using a single section interaction structure is in the final assembly phase as proof of concept with about 2 W output power. The E-band TWT performance will open new perspectives in the availability of long range wireless links with multi-Gb/s data rate needed for enabling 5G and 6G new networks.

Index Terms— **E-band, Traveling Wave Tube, Double Corrugated Waveguide, Wireless link**

I. INTRODUCTION

E- band (71 - 76 GHz and 81 - 86 GHz) is of high interest having 10 GHz band allowed for wireless communications in point to point (PtP) [1]–[3]. High data rate links are fundamental for high capacity data distribution in support of 5G and 6G (G is generation) concepts. E-band links are commercially available with data rate of a few gigabits per second (Gb/s) depending on the atmospheric conditions. However, the relatively low power of solid state amplifiers, in the range of 1 Watt per module, has to be compensated by high gain antennas to achieve range and Signal-to-Noise (SNR) ratio to satisfy the link budget for the typical availability of 99.99% in the rain zone of operation [4]–[6]. High gain antennas have relatively large footprint. In addition, if links with tens of Gb/s are needed, a cluster of front-ends has to be used with a combined large footprint that makes difficult to find sites for its installation [7]. The availability of higher transmission power would enhance the spectral efficiency with increased data rate for the same frequency band and reduce the antenna footprint, making front-ends more compact and easier to deploy.

Traveling wave tubes (TWTs) are the only devices able to provide tens of Watt at millimeter waves with compact dimensions [8]. Their working mechanism is based on the transfer of energy from an electron beam to a RF signal propagating in a guiding structure or slow wave structure (SWS) in high vacuum. The SWS reduces the wave phase velocity to be synchronized with the velocity of the electrons of the beam. The dimensions of the SWS are a function of the wavelength. The short wavelength at E-band makes very difficult the fabrication of helix slow wave structures, typical of microwave TWTs. Only one helix TWT space qualified is reported operating up to 75 GHz [9]. Different SWSs based on metal waveguides have been introduced, easier to manufacture than helices, with the dimensions to support E-band frequencies, such as the folded waveguide [10] or the double corrugated waveguide [11].

Also in case of metal SWSs, the short wavelength at millimeter waves makes the fabrication challenging due to the tight tolerance and the dimensions of the smallest features. The use of 3D electromagnetic simulators and high computation power provided by GPUs have substantially improved the TWT design permitting more accurate simulation domain for modeling the interaction mechanism. However, accuracy of fabrication, tolerance, assembly and surface roughness of the SWS metal walls are crucial elements for the successful production of TWTs, but can be only partially included in simulations [12].

E-band TWTs [1], [10], [13]–[16] have been investigated mostly for space applications. Only a few prototypes were produced and tested. A folded waveguide E-band TWT was reported with more than 40 W output power and 38 dB gain [10]. A MPM (microwave power module) module including a 81 - 86 GHz serpentine TWT with 200 W output power is reported in [14].

TWTs are presently used in niche applications, such as space and defence, where cost is not a primary parameter. One of the most important features requested to TWTs to be adopted in the wireless system market is to be affordable and of simple fabrication for high volume production. The double corrugated waveguide (DCW) has been demonstrated to be of relatively easy fabrication in a broad range of frequencies up to 1 THz due to its simple structure and alignment of the parts.

This paper presents the first ever fabricated 71 - 76 GHz TWT for wireless communications based on the double corrugated waveguide. The TWT is designed to provide about 70W saturated output power and more than 35 dB gain. Its simple structure and performance will permit to enable future long links with multi-Gb/s data rate in point to point and also wide area coverage with low gain antennas.

This paper is organized as follows. Section II reports the design and simulation of the DCW and the main parts of the E-band TWT. Section III describes the fabrication of the TWT's parts, including a detailed description of the CNC milling and diffusion bonding processes for manufacturing the DCW circuit.

II. TWT DESIGN

The E-band TWT specifications are defined on the basis of a deployment scenario, relevant for 5G and 6G networks [2], [17], to provide multi Gb/s high data rate over long links with high modulation scheme, not achievable by the actual E-band front ends powered by solid state amplifiers. The range is a function of transmission power and antenna gain. However, there is a limit in the level of achievable antenna gain. Only higher transmission power can compensate it. Range also depends on the availability. E.g.

99.99% availability in ITU zone K (42 mm/h) adds about 12 dB/km attenuation to the link budget at E-band. The data rate for a given range is a function of the SNR to enable the required modulation scheme. To consider that higher modulation schemes need high linearity with the need to operate at 6 - 9 dB back-off. If a channel with 1 GHz bandwidth is considered, it is possible to achieve about 6 Gb/sec per channel by 256 QAM (Quadrature Amplitude Modulation) modulation scheme (requirements: 9 dB back-off and SNR about 35 dB), with about 6 bits/s/Hz real spectral efficiency (assuming 0.75 Forward Error Correction - FEC). As a good estimate, the link budget for this data rate and a link 1.5 km long, suitable for transport of high capacity, by using small diameter 39 dBi antennas, assuming 5 dB low noise amplifier at the receiver, requires about 65 - 70 W saturated power. On that basis, the E-band TWT specifications are set to enable wireless links to satisfy those specifications. The TWT is designed to provide about 70 W output power and more than 35 dB gain in the 71 - 76 GHz band.

In the following, the design and simulation by 3D simulator (CST MWS [18]) of the main the parts of the TWT will be discussed.

A. Double Corrugated Waveguide

A double corrugated waveguide (DCW) was designed in the 71 - 76 GHz band with phase velocity synchronised with a 12.2 kV beam voltage. This beam voltage is relatively low to be generated by a compact power supply. The DCW was designed including both rectangular and triangular pillars (schematic in Fig. 1). The dimensions of the rectangular and triangular pillars DCW used in the circuit are listed in Table I. The dispersion curve for both rectangular and triangular pillars DCW are shown in Fig. 2. A slightly different period (1125 microns) was used for the square pillar DCW to have the same synchronism at 12.2 kV to compare the interaction impedance for the same beam voltage. The beam line related to the beam voltage (13.05 kV) used in the Particle in cell simulations (PIC) is also shown. An average interaction impedance higher than 3.5 Ω over the full band is obtained for the triangular pillar DCW (Fig. 3). To note that the interaction impedance of the triangular pillar DCW is about two times the interaction impedance of the square pillars DCW [19]. However, the square pillar DCW is used in the coupler, where there is no interaction with the electron beam.

The general topology of one section DCW interaction circuit, that can be used as first or second section in single or two sections TWT, including the couplers to the WR-10 flanges, is shown in Fig 4. The second port could be either the idle port of the sever in the input section or the output port of the second section. The number of periods depends on the design specifications. The interaction region consists of triangular pillars, while the couplers are made by square pillars. The triangular pillars offer higher interaction impedance, but are more difficult to fabricated. For this reason their use is limited in the interaction region. The scope of the couplers is to transform the hybrid mode in the DCW in a TE_{01} mode. Since there is no interaction with the electron beam, the rectangular pillars, easier to fabricate, have been used. Each coupler includes 15 rows of pillars tapered in height to match the WR-10 flange. The S-parameters of a DCW circuit with 45 periods in the interaction region and 15 periods for each coupler, are shown in Fig. 5. To note the wide band of the DCW. A reduced copper conductivity is set in the simulation process ($\sigma = 3.9 \times 10^7$ S/m).

Typically, a TWT needs two sections of interaction structure separated by a sever to satisfy the gain specification [1]. The sever is a region between the two sections where there is no transmission of RF signal to avoid oscillations. The E-band TWT sever consists of output port of the first section and the input port of the second section
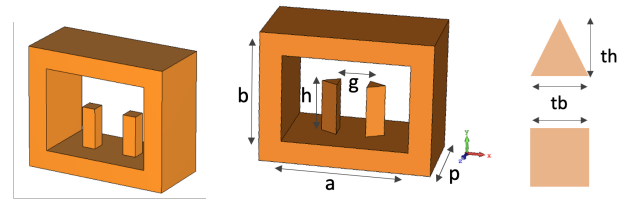

Fig. 1.　(Left) Square Pillar DCW; (center) Triangular Pillar DCW; (right) pillar section

TABLE I
DCW DIMENSIONS (MICRONS)

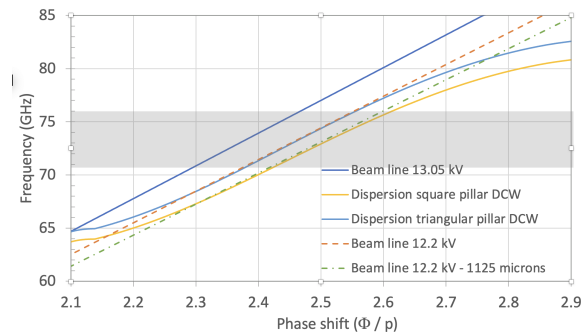|	
Beam tunnel width (g)	300
Square pillar width (tb)	200
Triangular pillar base (tb)	200
Triangular pillar height (th)	200
Pillar height (h)	680
Period (p)	1100
Waveguide height (b)	1270
Waveguide width (a)	1680
Beam radius	130
Input/ Output Port Flanges	WR 10

Fig. 2.　Dispersion the triangular pillar DCW as a function of frequency, with superimposed beam lines (12.2 kV and 13.05 kV and 12.2 kV with the period of the square pillar DCW).

terminated by high absorbing material. The frequency information is transferred to the second section by the modulated electron beam. The electron beam has been set with 90 mA current, confined by a magnetic field of about 0.4 T, generated by a conventional permanent periodic magnetic system (PPM).

The E-band TWT was initially designed with two sections to meet the specification. The first section comprises 30 periods to provide about 19 dB gain, the output section includes 60 periods for satisfying the gain and power specifications. The total length of the interaction region is about 100 mm. The PIC simulations demonstrate a gain better than 37 dB (Fig. 6) and an output power of about 70 W with 10 mW input power (Fig. 7). The Pin-Pout curve (Fig. 8) shows the linear zone of the output power curve to operate the TWT. The two-sections TWT was simulated including a sever with the two idle ports, that will be fabricated with graphite absorber at the end. As a reference, to compare the improvement provided by the use of the triangular pillars, a double section DCW TWT with square pillars, with 40 periods in the first section and 90 periods in the second section, produces only 30 dB gain. The PIC simulations were performed by a workstation with GPU, with a computational domain with about 10M mesh cells and 2M particles.

As first TWT prototype, it was decided to first build a TWT identical to the two-section TWT, but with one section. This permits to test the full fabrication process of the TWT, with the advantage of
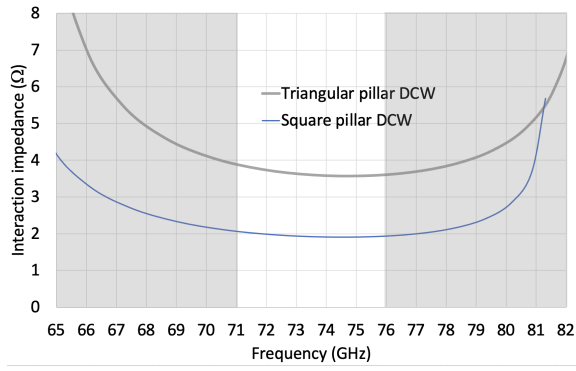
Fig. 3.　Interaction impedance of the triangular pillar and square pillar DCW as a function of frequency.
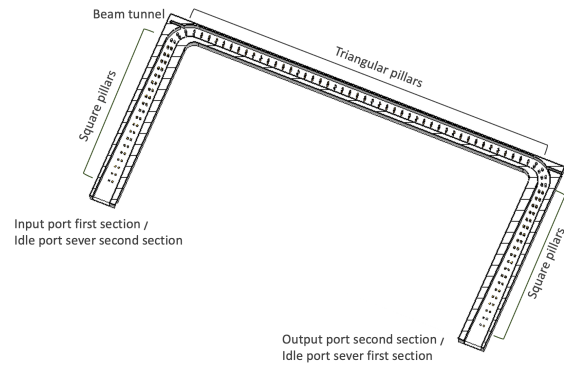

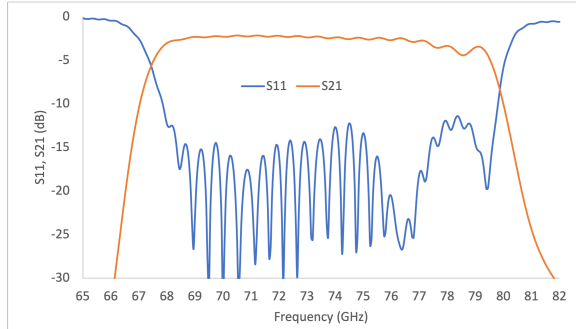Fig. 4.　General DCW circuit with interaction region and couplers.

Fig. 5.　S-parameters of a DCW circuit with 45 periods as in Fig 4.

a short interaction region to reduce the effort for the beam alignment and magnetic focusing. A one section with 45 periods triangular pillar DCW interaction structure has been designed to provide about 22 dB gain (Fig. 9) and more than 1.5 W output power (Fig. 10) with 10 mW input power. These values are low enough to avoid possible oscillations. The different behavior of output power as a function of the frequency between the two sections TWT (Fig. 7) and the single section TWT (Fig. 10) is due to a slight change in the interaction conditions. The single section TWT is fed by the RF signal. The second section of the two sections TWT is fed by a beam already modulated that determines a change in the synchronism conditions at higher frequency.

B. Electron optics, collector and RF windows

The electron gun was designed to produce a beam with 130 μm radius and 90 mA current. The same structure of the electron gun in [20] was used with slightly modifications to the anode shape and
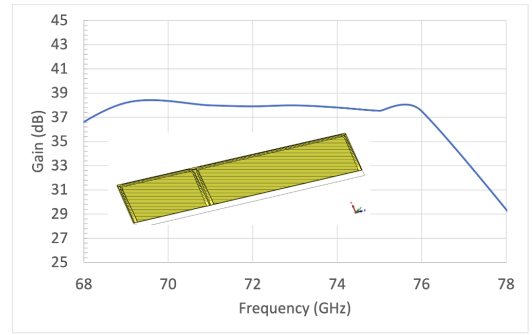

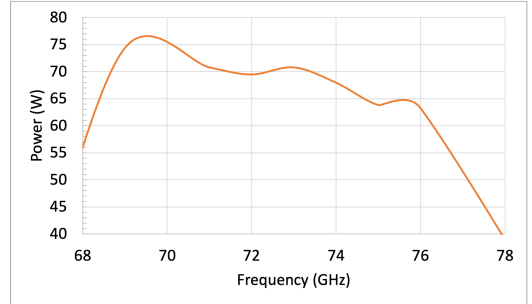Fig. 6.　Gain of the two sections DCW TWT (inset: simulation domain).

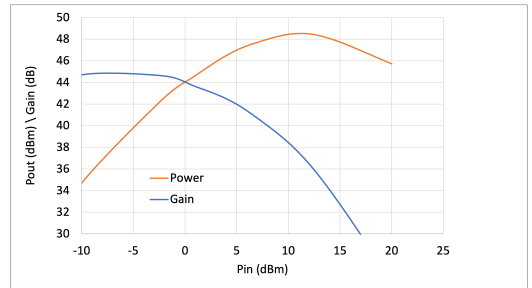Fig. 7.　Output power of the two sections DCW TWT.
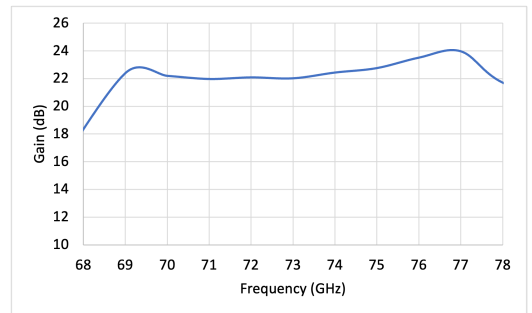

Fig. 8.　Pin-Pout of two sections DCW TWT.

Fig. 9.　Gain of the one section DCW TWT.

dimensions. A permanent periodic magnetic system was designed to produce 0.4 T (Fig. 11) over the full length of the interaction structure. Samarium Cobalt magnets (Sm_2Co_{17}) with Br 1.13T are used. The collector is a single stage collector with possibility to have depression. The optimization of the efficiency by a multistage depressed collector will be considered as future development. The RF Windows are conventional pill box cavities with an Alumina dielectric layer. The simulation of the RF window S-parameters is shown in Fig. 12. To note that the S_{11} is well below -15 dB over the
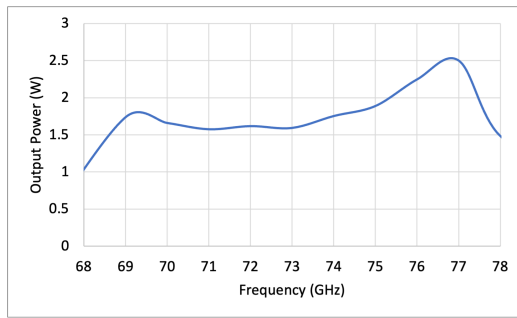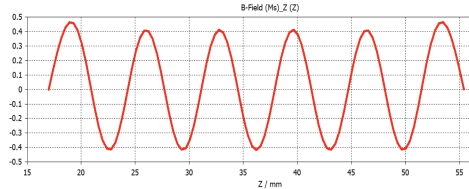
Fig. 10. Output power of the one sections DCW TWT.

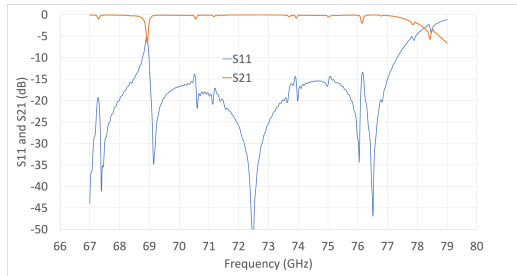Fig. 11. Longitudinal magnetic field (0.4 T) produced by the PPM system.

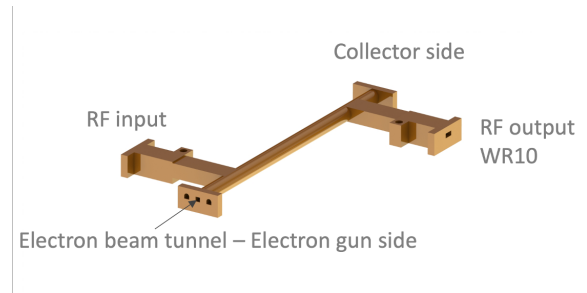Fig. 12. Simulated S-parameter of the RF window.

Fig. 13. Drawing of the final structure of the single section DCW circuit.
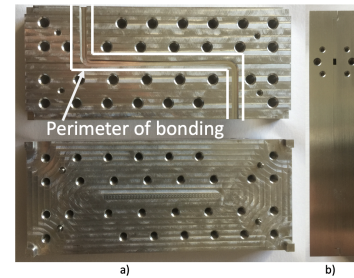
Fig. 14. Typical split block approach a) split blocks, b) assembled for bonding [1].

full bandwidth. The low S_{11} out of the band, at about 69 GHz, is not critical for the single section TWT also due to the low power generated.

III. E-BAND TWT FABRICATION

In this section the main fabrication aspects of the most relevant TWT parts will be discussed. In particular, a new technique to overcome the risk of eventual weak diffusion bonding for assembling the DCW circuit will be described.

A. Double corrugated waveguide circuit fabrication

The double corrugated waveguide circuit includes the input and output couplers with the flanges for connecting the RF windows and the electron gun and collector to the beam tunnel. The circuit is built by two split blocks made of Oxygen Free High Conductivity (OFHC) copper. One block includes the waveguide with pillars, the couplers and beam tunnel. The fabrication of this block requires high accuracy computer numerical control CNC milling and very small diameter toolings (a few hundreds of microns). The second block is a flat lid to close the waveguide. The surface roughness of the metal walls should be ideally below the skin depth (240 nm at 76 GHz) to ensure low ohmic losses. This level of surface finishing (about 200 -300 nm) is achieved by using very high spindle speed (50000 rpm) CNC milling [12], [21].

The two blocks are assembled and sealed together by diffusion bonding. Diffusion bonding is a process that permits to restore the

atomic bonding of two or more metal parts by applying high pressure at temperature close to the melting point of the metal to bond. This process ensures a vacuum tight sealing of the circuit. After diffusion bonding, the resulting block is machined by CNC milling to achieve the shape suitable to support the permanent magnetic focusing system. The drawing of the final single-section DCW circuit after CNC milling to be assembled in the TWT is shown in Fig 13. The cylindrical region of the barrel has a diameter of 4 mm.

This final machining phase of the bonded block could be critical. Fig. 14 shows a typical split blocks structure for diffusion bonding [1]. The circuit is machined in two blocks. The bonding has to be achieved over the full surface of contact. However, the region where the bonding has to be strong and vacuum tight is along the perimeter of the waveguide. If the bonding is not strong or incomplete along the perimeter defined by the waveguide walls and the beam tunnel, it could lead to fractures of the material or deformations during the machining, that make unusable the circuit and requires to fabricate a new circuit with high additional costs. After diffusion bonding there is no simple way to check the quality of the bonding in the perimeter of the final structure to be machined. This makes uncertain the final machining and its successful completion without damaging the delicate final structure.

To resolve this problem, a new shaped split blocks structure is adopted. The two blocks of the DCW circuit are shaped with a geometry very close to the final shape of the barrel. Fig. 15 shows the realized two parts, the waveguide block and the flat lid, of the E-band DCW. The figure shows the pillars, the couplers and the beam tunnel. Fig. 16 shows a detail of the triangular pillars inside the waveguide. The alignment is obtained by dowel pins. To note the high fabrication quality. The total length of each block is about 80 mm including the interaction region (about 50 mm) and the beam tunnel with the flanges to connect to the electron gun and the collector. The profile of the two parts is slightly wider than the final geometry to have the metal walls with sufficient thickness for the final CNC milling. This geometry permits, after the diffusion bonding, to assess the quality of the bonding at the interface over the full perimeter and eventually
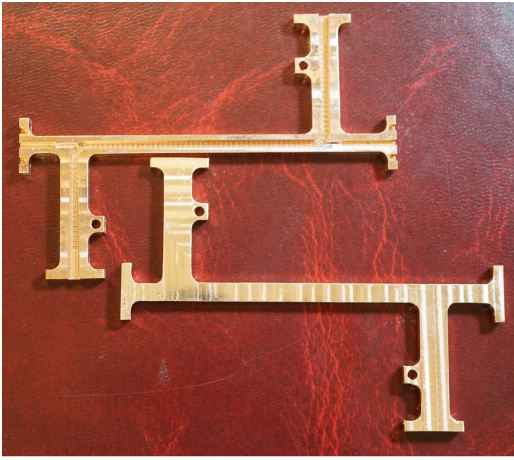
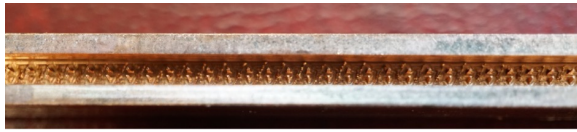Fig. 15.   Two blocks of the DCW circuit to be assembled by diffusion bonding.

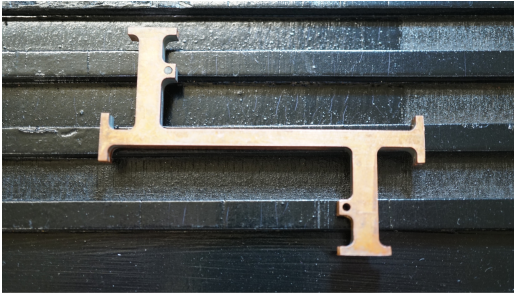Fig. 16.   Detail of the triangular pillars in the interaction region.

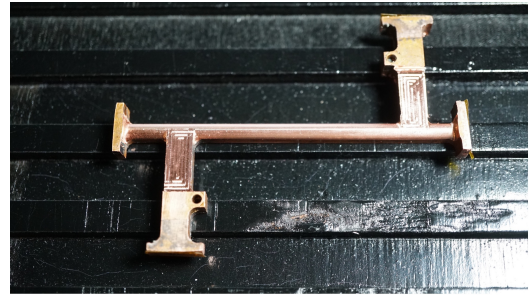Fig. 17.   DCW circuit after diffusion bonding.

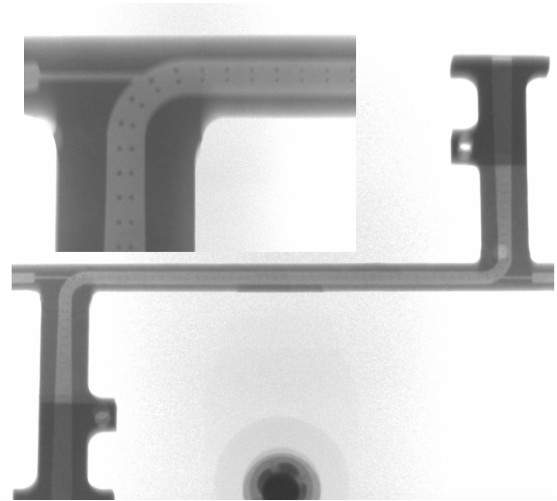Fig. 18.   Final barrel after final CNC milling machining.

Fig. 19.   X-rays CT scan images of the bonded DCW circuit. (Upper) detail of the bend, (Lower) full DCW circuit.
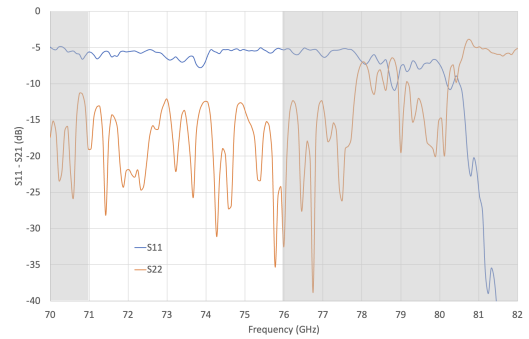

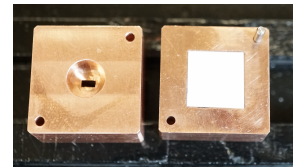Fig. 20.   Measured S-parameters of the DCW circuit after diffusion bonding.

Fig. 21.   RF window blocks: cavity (left); Alumina sheet (right).

reinforce the region of weak bonding or vacuum leakage by an additional brazing step. The diffusion bonding of the two blocks, due to the delicate metal structure, requires a careful definition of pressure and temperature to avoid deformations of the structure. For the structure here discussed, 10 kN pressure was applied with 1000° C temperature.

Fig. 17 shows the two blocks after diffusion bonding. This circuit was inspected and successfully tested for vacuum leakage. A further CNC milling of the circuit was then performed for achieving the final shape as shown in Fig. 18. The longitudinal barrel has a circular section of 4 mm diameter to be assembled with the PPM system. The two lateral flanges will be connected to the RF windows. The beam tunnel is connected to the electron gun and collector by flanges using dowel pins for a high accuracy alignment.

Fig. 19 shows the X-ray CT scan of the bonded DCW circuit. To note the quality of the bonding and the lack of any deformation after diffusion bonding.

Fig. 20 shows the measured S_{11} and S_{21} of the DCW circuit after diffusion bonding. The measurement was taken connecting the input and output ports as in Fig. 18 directly to the extender flanges, slightly reducing the accuracy.

B. RF Windows

The fabrication of the RF window is performed by CNC milling of two blocks with an identical half cavity. The first block has a flange to connect to the corresponding flange of the DCW block (Fig 13). The second block has the WR10 flange on one side and the frame to support the ceramic sheet in the other side (Fig. 21). The first
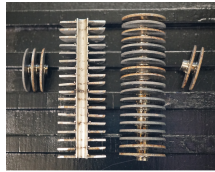
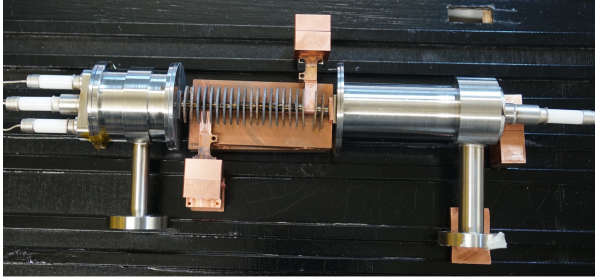Fig. 22. Pole piece assembly for the PPM stack.

Fig. 23. Fabricated E-band TWT assembled, not sealed (without the magnets).

block is brazed to the DCW circuit. Then the second block with the Alumina sheet is brazed to the first block.

C. Permanent Periodic Magnetic System

The permanent periodic magnetic (PPM) system consists of iron pole pieces alternate with magnets. The iron pole pieces are built in two halves. They are laser welded to a stainless steel pipe that encloses the DCW circuit. The stainless steel pipe is divided in two halves along the axis to be assembled around the barrel and then welded. The scope of the pipe is also to provide a robust support to the delicate copper structure (Fig. 22).

D. E-band TWT Assembly

The assembly of the parts of the TWT is in the final stage. The DCW circuit has been brazed with the RF windows. Unfortunately, a residual of brazing material leaked in the beam tunnel. The beam tunnel was mechanical cleaned, but to avoid the risk of particles inside the DCW, a new DCW and RF windows were built and will be assembled. The collector and the electron gun have been fabricated and will be assembled to the DCW circuit by laser welding. After this assembly phase, the TWT will be baked to achieve a vacuum level better than 10^{-8} torr for the correct operation. Finally, measurements of the beam transmission and RF output will be performed. Fig. 23 show the TWT as it will be after the assembly.

IV. CONCLUSIONS

The design and fabrication of a novel E-band TWT demonstrates the feasibility of a low cost TWT for enabling long range in E-band links. The simple structure of the TWT permits to reduce costs and is suitable for a large scale production for deployement in new 5G and 6G high capacity networks. The next step will be the assembly vacuum tight of the TWT and the measurement of performance. Those measurements will be the basis for the fabrication of the two stages TWT with full performance.

V. AKNOWLEDGMENT

REFERENCES

[1] X. Li, X. Huang, S. Mathisen, R. Letizia, and C. Paoloni, "Design of 71-76 ghz double-corrugated waveguide traveling-wave tube for satellite downlink," *IEEE Transactions on Electron Devices*, vol. 65, no. 6, pp. 2195–2200, 2018.

[2] C. Dehos, J. L. González, A. De Domenico, D. Kténas, and L. Dussopt, "Millimeter-wave access and backhauling: the solution to the exponential data traffic increase in 5g mobile communications systems?," *IEEE Communications Magazine*, vol. 52, no. 9, pp. 88–95, 2014.

[3] U. J. Lewark, J. Antes, J. Walheim, J. Timmermann, T. Zwick, and I. Kallfass, "Link budget analysis for future e-band gigabit satellite communication links (71–76 and 81–84 ghz)," *CEAS Space Journal*, vol. 4, no. 1, pp. 41–46, 2013.

[4] A. M. Al-Samman, M. Mohamed, Y. Ai, M. Cheffena, M. H. Azmi, and T. A. Rahman, "Rain attenuation measurements and analysis at 73 ghz e-band link in tropical region," *IEEE Communications Letters*, vol. 24, no. 7, pp. 1368–1372, 2020.

[5] C. Han and S. Duan, "Impact of atmospheric parameters on the propagated signal power of millimeter-wave bands based on real measurement data," *IEEE Access*, vol. 7, pp. 113626–113641, 2019.

[6] L. Manoliu, R. Henneberger, A. Tessmann, J. Seidel, M. Eppard, and I. Kallfass, "Impairments of atmospheric attenuation on a wideband e-band outdoor communication link," in *2021 51st European Microwave Conference (EuMC)*, pp. 990–993, 2022.

[7] F. André, J.-C. Racamier, R. Zimmermann, Q. Trung Le, V. Krozer, G. Ulisse, D. F. G. Minenna, R. Letizia, and C. Paoloni, "Technology, assembly, and test of a w-band traveling wave tube for new 5g high-capacity networks," *IEEE Transactions on Electron Devices*, vol. 67, no. 7, pp. 2919–2924, 2020.

[8] C. Paoloni, D. Gamzina, R. Letizia, Y. Zheng, and N. C. L. Jr., "Millimeter wave traveling wave tubes for the 21st century," *Journal of Electromagnetic Waves and Applications*, vol. 35, no. 5, pp. 567–603, 2021.

[9] N. R. Robbins, D. R. Dibb, W. L. Menninger, X. Zhai, and D. E. Lewis, "Space qualified, 75-watt v-band helix twta," in *IVEC 2012*, pp. 349–350, 2012.

[10] S. Liu, Q. Xie, Z. Chen, Y. Wu, Z. Zi, X. Wu, J. Cai, and J. Feng, "High linear power e-band traveling-wave tube for communication applications," *IEEE Transactions on Electron Devices*, vol. 68, no. 6, pp. 2984–2989, 2021.

[11] M. Mineo and C. Paoloni, "Double-corrugated rectangular waveguide slow-wave structure for terahertz vacuum devices," *IEEE Transactions on Electron Devices*, vol. 57, no. 11, pp. 3169–3175, 2010.

[12] D. Gamzina, H. Li, L. Himes, R. Barchfeld, B. Popovic, P. Pan, R. Letizia, M. Mineo, J. Feng, C. Paoloni, and N. C. Luhmann, "Nanoscale surface roughness effects on thz vacuum electron device performance," *IEEE Transactions on Nanotechnology*, vol. 15, no. 1, pp. 85–93, 2016.

[13] Z. Zi, S. Liu, Q. Xie, S. Li, J. Cai, and S. Zhao, "A 70w 81-86ghz e-band cw travelling wave tube," in *2019 International Vacuum Electronics Conference (IVEC)*, pp. 1–2, 2019.

[14] R. Kowalczyk, A. Zubyk, C. Meadows, T. Schoemehl, R. True, M. Martin, M. Kirshner, and C. Armstrong, "High efficiency e-band mpm for communications applications," in *2016 IEEE International Vacuum Electronics Conference (IVEC)*, pp. 1–2, 2016.

[15] R.-J. Hwu, D. K. Kress, S. V. Judd, J. M. Krebs, and L. P. Sadwick, "81–86 ghz e-band 90 watts high power traveling wave tubes," in *2016 IEEE International Vacuum Electronics Conference (IVEC)*, pp. 1–2, 2016.

[16] C. Robertson, A. Cross, C. Gilmour, D. Dyson, P. G. Huggard, F. Cahill, M. Beardsley, R. Dionisio, and K. Ronald, "71-76 ghz folded waveguide twt for satellite communications," in *2019 International Vacuum Electronics Conference (IVEC)*, pp. 1–2, 2019.

[17] C. Paoloni, "Sub-thz wireless transport layer for ubiquitous high data rate," *IEEE Communications Magazine*, vol. 59, no. 5, pp. 102–107, 2021.

[18] "Cst studio suite (microwave studio)," 2018.

[19] M. Mineo and C. Paoloni, "Improved corrugation cross-sectional shape in terahertz double corrugated waveguide," *IEEE Transactions on Electron Devices*, vol. 59, no. 11, pp. 3116–3119, 2012.

[20] R. Basu, J. M. Rao, R. Letizia, and C. Paoloni, "Low cost electron gun for d-band traveling wave tubes," in *2021 22nd International Vacuum Electronics Conference (IVEC)*, pp. 1–2, 2021.

[21] D. Gamzina, L. G. Himes, R. Barchfeld, Y. Zheng, B. K. Popovic, C. Paoloni, E. Choi, and N. C. Luhmann, "Nano-cnc machining of sub-thz vacuum electron devices," *IEEE Transactions on Electron Devices*, vol. 63, no. 10, pp. 4067–4073, 2016.